Original Article

Small field dose delivery evaluations using cone beam optical computed tomography-based polymer gel dosimetry

Timothy Olding[1], Oliver Holmes[1], Paul DeJean[1], Kim B. McAuley[2], Ken Nkongchu[3], Giles Santyr[4-6], L. John Schreiner[1,7,8]

[1]Department of Physics, [2]Department of Chemical Engineering, Queen's University, Kingston, Ontario, Canada, [3]Henry Ford Hospital, Detroit, MI, USA, [4]Imaging Research Laboratories, Robarts Research Institute, London, ON, Canada, [5]Department of Medical Biophysics, [6]Department of Medical Imaging, University of Western Ontario, London, ON, Canada, [7]Department of Oncology, Queen's University, Kingston, Ontario, [8]Department of Medical Physics, Cancer Centre of Southeastern Ontario at Kingston General Hospital, Kingston, Ontario, Canada

Received on: 07.07.10 **Review completed on: 07.08.10** **Accepted on: 05.11.10**

ABSTRACT

This paper explores the combination of cone beam optical computed tomography with an *N*-isopropylacrylamide (NIPAM)-based polymer gel dosimeter for three-dimensional dose imaging of small field deliveries. Initial investigations indicate that cone beam optical imaging of polymer gels is complicated by scattered stray light perturbation. This can lead to significant dosimetry failures in comparison to dose readout by magnetic resonance imaging (MRI). For example, only 60% of the voxels from an optical CT dose readout of a 1 l dosimeter passed a two-dimensional Low's gamma test (at a 3%, 3 mm criteria, relative to a treatment plan for a well-characterized pencil beam delivery). When the same dosimeter was probed by MRI, a 93% pass rate was observed. The optical dose measurement was improved after modifications to the dosimeter preparation, matching its performance with the imaging capabilities of the scanner. With the new dosimeter preparation, 99.7% of the optical CT voxels passed a Low's gamma test at the 3%, 3 mm criteria and 92.7% at a 2%, 2 mm criteria. The fitted interjar dose responses of a small sample set of modified dosimeters prepared (a) from the same gel batch and (b) from different gel batches prepared on the same day were found to be in agreement to within 3.6% and 3.8%, respectively, over the full dose range. Without drawing any statistical conclusions, this experiment gives a preliminary indication that intrabatch or interbatch NIPAM dosimeters prepared on the same day should be suitable for dose sensitivity calibration.

Key words: Cone beam optical computed tomography, polymer gel dosimetry, small field dose delivery, three dimensional

Introduction

Since gel dosimetry first emerged as a prospective candidate for high resolution, three-dimensional (3D) dose measurements in radiation therapy, a number of systems have been employed for readout of gel dose. These systems have primarily been based on the imaging modalities of magnetic resonance imaging (MRI or MR imaging),[1,2] optical computed tomography (CT),[3] and X-ray CT,[4,5] each of which has its disadvantages and advantages. Optical CT, in particular, has the disadvantage of stray light perturbation affecting optical dose readout accuracy.[6,7] However, this modality also has a key advantage of accessibility in most clinical environments, as these scanners are low cost, compact and usually portable.[8,9] In addition, fast 3D imaging has been realized through the use of either a cone beam[10,11] or parallel beam[12-14] charge-coupled device (CCD) optical scanner configuration. The much reduced imaging time of these area detection-based scanners is an important step forward toward the use of Fricke-based gels for 3D dosimetry, which are limited

Address for correspondence:
Dr. Timothy Olding,
Department of Medical Physics,
Cancer Centre of Southeastern Ontario at Kingston General Hospital, 25 King Street West, Kingston, Ontario K7L 5P9, Canada.
E-mail: tim.olding@krcc.on.ca

Access this article online

Quick Response Code:

Website: www.jmp.org.in

DOI: 10.4103/0971-6203.75466

by diffusion-related loss of spatial dose integrity over time.[15,16]

The performance capabilities of the commercially available Vista™ cone beam optical CT scanner (Modus Medical Devices Inc, London, ON, Canada) have been investigated and found to be suitable for readout of optically absorbing gel dosimeters.[17] The Fricke-xylenol orange-gelatin (FXG) absorbing gel dosimeter, in particular, can be employed for 3D verification of intensity modulated radiotherapy (IMRT) dose distributions.[10] However, diffusion effects in the FXG dosimeter, which have a reasonably small effect on spatial dose integrity throughout most of the imaged volume of IMRT dose distributions over time, become more problematic when examining high dose gradients such as those found in small field dosimetry. Post-imaging correction schemes become necessary in order to obtain accurate dose measurements.[18]

The focus of this investigation is to determine whether an optically scattering polymer gel dosimeter could be used in combination with cone beam optical CT for the evaluation of high gradient dose distributions such as those from small field deliveries. Polymer gels have high resolution dose contrast response and do not suffer from the diffusion effects found in the Fricke-based gels.[19,20] Hence, these gels should be appropriate for investigating small field dose distributions. However, cone beam optical CT readout of polymer gels has previously been shown to be significantly perturbed by contaminant stray light[17,21,22] that greatly affects the measurement accuracy of this approach.

The main task in this work is to establish whether the effects of stray light can be reduced or managed to the point where an acceptable dosimetric accuracy is achieved for small field deliveries to a polymer gel dosimeter imaged with the Vista cone beam optical CT scanner. This application may be of interest in situations where the dose delivery is extended in duration and where Fricke systems are not well suited for dose evaluation (e.g., small field irradiations with lower output or brachytherapy). The accuracy of this combination of gel dosimeter and readout method could be assessed by a comparison between reference (“true”) and measured (polymer gel-cone beam optical CT) dose distributions using dose difference maps. However, such maps are particularly sensitive to differences in the high dose gradients of the small field pencil beam delivery, since small spatial errors in either dataset can lead to large dose differences between the measured and planned distributions. A better comparison of spatial dose distributions can be obtained through use of Low’s gamma function,[23,24] which quantifies the agreement of the combined metrics of dose difference and distance-to-agreement between two dose distributions into a single “gamma” value. The gamma function assigns values less than 1 in regions where dose difference and distance-to-agreement are within set criteria, for example, 3% dose and 3 mm distance between points in the treatment planning system-calculated and gel-measured dose distributions. Values greater than 1 are understood as having failed the criteria. The goal for the evaluation of high dose gradients in this study was to achieve full (or near to full) high resolution voxel agreement between reference and measured dose distributions using 2% dose and 2 mm distance-to-agreement gamma function criteria. In this preliminary work, the Low’s gamma function tool was used primarily to provide a fast, quantitative measure of the dosimetry with optical CT readout before and after modification of the dosimeter.

An *N*-isopropylacrylamide (NIPAM)-based recipe[25] was employed in the preparation of all polymer gel dosimeters in this report. This formulation approach was originally developed as a lower toxicity alternative to the more widely used acrylamide-based polymer gel.[19,20] Results in this paper present an initial comparison of cone beam optical CT and MRI in the dosimetric readout of a test small field dose delivery to a NIPAM gel-filled standard-sized 1 l polyethylene terephthalate (PETE) jar dosimeter. Following this comparison is an independent assessment of the optical CT scanner using calibration hybrid acrylic-gelatin scattering gel phantoms. The use of these phantoms separates the measurement from the uncertainties of polymer gel dosimeter preparation and dose delivery. The NIPAM gel dosimeter formulation and preparation procedure are then evaluated and modified to match the scanner’s performance capabilities. Finally, the dosimetry of the improved formulation/preparation is evaluated and different calibration methodologies investigated for practical use.

Experiment

Gel preparation

Dosimeters in this study were prepared under atmospheric (normoxic) conditions according to one of two preparation procedures referred to as procedures A and B, which differ primarily in the mixing order of chemicals and temperature at the time of NIPAM monomer addition. The reason for the investigation of two different preparation procedures will be discussed in a latter section. In procedure A, gels containing 5 wt% gelatin (300 bloom Type A porcine gelatin, Cat. No. G2500, Sigma-Aldrich Ltd, Oakville, Canada), 3 wt% *N*,*N*’-methylene-bis-acrylamide (BIS) cross-linking monomer (Cat. No. 146072, Sigma-Aldrich Ltd.), 3 wt% *N*-isopropylacrylamide (NIPAM) monomer (Cat. No. 415324, Sigma-Aldrich Ltd.), and 10 mM of tetrakis hydroxymethyl phosphonium chloride (THPC, Cat. No. 404861, Sigma-Aldrich Ltd.) in aqueous solution, were prepared according to a standard approach reported in

literature.[25] These polymer gels are henceforth identified according to literature convention as 6 %T, 50% C NIPAM, where T refers to the total weight percent of monomer, and C is the percentage of cross-linking monomer in the gel. As all dosimeters in this report have a cross-linking monomer percentage of 50%, the 50% C designation is assumed from this point forward. The gelatin was allowed to swell in 80 wt% of the total amount of de-ionized water at room temperature for 15 min and the solution was then heated to 50 °C while stirring. BIS cross-linker was added under stirring and the solution temperature held at 50 °C until the cross-linker was fully dissolved. The solution was allowed to cool to approximately 37 °C and the NIPAM monomer was added under stirring until the monomer was dissolved. A dilute solution of THPC antioxidant was prepared with the remaining 20 wt% of the water and added to the solution at a temperature of approximately 35 °C. The solutions were poured into 1 l PETE jars and refrigerated for 24 h prior to irradiation.

In the alternative approach (procedure B), polymer gel dosimeters with total monomer concentrations between 3–6 %T were prepared by allowing 5 wt% of gelatin to swell in 70 wt% of the de-ionized water at room temperature for 10 min and heating the solution to 50 °C as before. The BIS cross-linker was added under stirring at 50 °C until dissolved. The BIS–gelatin–water solution was then cooled to 34 °C. Separately, the NIPAM monomer and THPC were dissolved in the remaining water at room temperature. The NIPAM–THPC water solution was then added to the cooled BIS–gelatin–water solution, mixed for 1–2 min then poured into 1 l PETE containers, and refrigerated for 24 h prior to irradiation. The 3 %T, 3.5 %T, 4 %T, and 6 %T dosimeters contained 5, 5.83, 6.67, and 10 mM of THPC, respectively.

Gel irradiations

An initial comparison of the polymer gel imaging capabilities of cone beam optical CT and MRI was completed by using both modalities to image the same irradiated NIPAM dosimeter. A 6 %T cylindrical PETE jar dosimeter (with outer container diameter of 9.2 cm) prepared according to procedure A (batch A1) was used in this investigation. This dosimeter was irradiated with a 500 cGy calibration distribution consisting of three pencil beams of different beam weights delivered in a well-defined "A" dose pattern [Figure 1a]. The dosimeter was also irradiated with a 25 field, 500 cGy "K" pattern used as an evaluation dose distribution [Figure 1b]. The calibration "A" and measurement "K" patterned pencil beam deliveries were forward planned with a modified Milan Bentley dose calculation algorithm.[26,27] The treatment plan dose distributions of these two ("A" and "K") pencil beam plans had been independently well characterized with ion chamber measurements and Monte Carlo calculations and verified in their accuracy to within 1% of the maximum dose.[26,27] Hence, the "A" and "K" treatment plans were used as 'gold standard' reference dose distributions in this investigation for evaluation of gel dosimeter performance. Ultimately, of course, the intent would be to use gel dosimetry as the 3D validation tool, for example, in the commissioning of a treatment planning system. In this study, however, the gel dosimeter was the system being validated through use of the two independently well-characterized treatment plans.

The plans were delivered to the dosimeter through use of an in-house tomotherapy benchtop with pencil beam collimation customized to a T780C cobalt-60 radiotherapy unit (Best Theratronics, Kanata, ON), shown in Figure 1c. Pencil-beam collimation was realized by mounting a $7 \times 7 \times 7$ cm^3 Cerrobend block with a 0.65×0.65 cm^2 hole through its centre on the Co-60 unit. This collimated the beam to a 1×1 cm^2 field size at the isocentre of the gantry, located at a source-to-axis distance (SAD) of 80 cm. The irradiation of a single slice was achieved by rotating and translating the gel dosimeter on the stepper motor-controlled stage. As in serial tomotherapy, the gel phantom was advanced to the next slice (vertical height position) after one complete rotation. The irradiated dosimeter [Figure 1d] containing two "A" calibration distribution and one "K" measurement distribution was imaged ~12 h after delivery using optical CT, and on a subsequent day using MRI.

Deviations in beam output of the small fields (beam calibration errors or output numbers) or machine failure may not be picked up during the 3D gel dosimetry experiment using this internal calibration method. For this

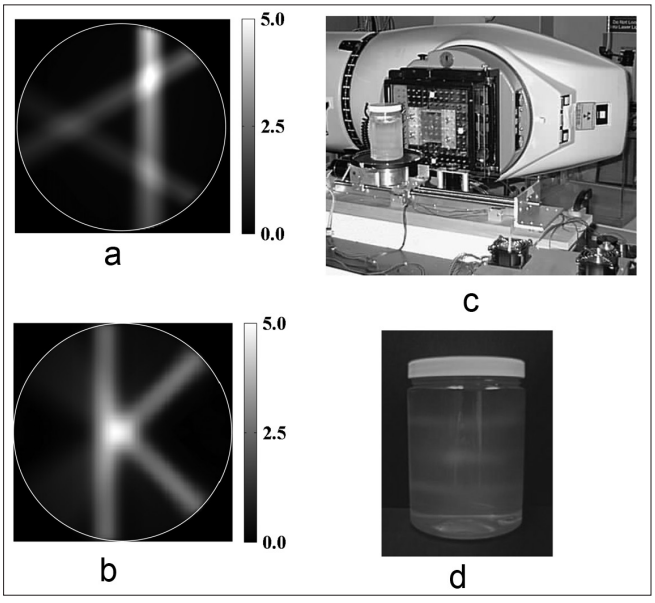

Figure 1: (a and b) Test 500 cGy "A" and "K" patterned pencil beam treatment plans. (c) The tomotherapy benchtop apparatus used to perform the pencil beam deliveries. (d) An irradiated NIPAM gel dosimeter

set of experiments though, a well-understood tomotherapy apparatus with fixed collimation and well-known dose rate (radioactive decay of the Co-60 source) were employed, so this was not anticipated to be a significant issue.

To evaluate the changes in formulation (%T monomer reduction) and preparation procedure (to procedure B), test "A" and "K" dose distributions were similarly delivered to four dosimeters prepared according to procedures B with monomer concentrations of 6 %T, 6 %T, 4 %T, 3.5 %T, and 3 %T (batches B1-B5, respectively) and imaged using optical CT. The calibration "A" dose delivery and test "K" delivery were separated by a vertical distance of 3.75 cm to ensure that the scattered dose affecting the adjacent planar dose delivery was minimal. Finally, different calibration approaches were assessed by delivering intersecting pencil beam "A" patterns at different heights in four 4 %T NIPAM gel dosimeters prepared in two batches (two dosimeter jars per batch) according to procedure B (batches B6 and B7, respectively) and imaged using optical CT.

Optical CT imaging

Optical readout of the dosimeters was completed under room temperature conditions at an illumination wavelength of 633 nm and camera lens aperture of f5 in the Vista cone beam optical CT scanner. A full description of the imaging and reconstruction process for the Vista scanner has previously been reported,[17] so only the necessary details are repeated here. Matching tank solution for the scanner consisted of a 12 wt% propylene glycol-in-water mixture, the refractive index of which (1.346 ± 0.001 at 590 nm) was monitored over time using a handheld refractometer with a central measurement wavelength of 589 nm (r^2 mini refractometer, Reichert Analytical Instruments, Depew, NY, USA) at room temperature (21 ± 1 °C). Room temperature measurements were taken using a digital temperature probe (TM99A-NA Digital Thermometer, Nuclear Associates, Carle Place, NY, USA).

Reference scans were completed on each dosimeter close to the time of irradiation, at the highest shutter exposure time possible without inducing camera pixel saturation, and the lowest gain setting. Data scans were acquired using the same camera settings as the reference scan at a post-irradiation time of ~12 h, unless otherwise specified. As the dosimeter reacts over a period of several hours after the irradiation,[25] the wait time of 12 h prior to optical CT scanning was chosen to ensure that the polymerization reaction was near completion at the time of imaging. For each scan, a set of 410 light intensity transmission projections were acquired over 360° in approximately 5–6 min. High resolution (0.5 × 0.5 × 0.5 mm^3 voxel) images, with a volume of 12.8 × 12.8 × 12.8 cm^3 incorporating the imaged dosimeter, were reconstructed in 10 min using a standard desktop computer.

MR imaging

MR imaging of the dosimeters was accomplished using an in-house built research scanner with a static magnet field strength of 1.89 T (Magnex Scientific, Abingdon, Oxon, England) and a 12 cm internal diameter transmit/receive birdcage coil (Morris Instruments, Inc., Ottawa, ON, Canada). The dosimeters were placed in the magnet room for 24 h prior to scanning to allow the gel time to reach room temperature. Centric *k*-space acquisition minimized the errors in spin–spin relaxation rate ($R2$) due to radiofrequency (RF) power deposition-related temperature increases, notably in the area of high dose gradients.[28] The phase of the refocusing 180° RF pulse was shifted by π for successive phase encode lines in order to place any centre-line artifacts (i.e., "zipper" artifacts) related to contamination of the spin-echo signal by stimulated echoes at the edges of the image for removal during post-processing.[29]

Thirty-two echoes were predicted to obtain a optimal dose resolution for the research scanner's echo spacing capability of 40 ms (the shortest attainable echo spacing without inducing significant artifacts) and the expected $R2$ range from gel readout (~1.50 to ~1.85 s^{-1}).[30-32] However, hardware/software constraints required the image acquisition to be limited to 26 echoes. We confirmed that the change to 26 echoes did not perturb measured $R2$ values through a series of separate experiments on gadolinium doped aqueous standards, with a range of $R2$s spanning the rates expected for the irradiated dosimeters. A 128 mm field of view was used and 17 slices were acquired with thicknesses of 5 mm each to give a spatial resolution of 1 mm × 1 mm × 5 mm, with two averages taken per scan. $R2$ maps were obtained by performing a pixel-by-pixel exponential fit to the image data.[33] As the research scanner exhibited distortions due to nonlinear gradients and static field inhomogeneities of up to 10 mm, a combined method adapted from two previous reports was employed to corrected these distortions to within 1 mm.[34,35] The measured distortions in all three orthogonal imaging directions (x,y,z) were fitted to a three-variable (x,y,z) third-order polynomial and then used to correct subsequent images acquired using the imaging system. The distortion mapping and correction used simple grid phantoms of approximately the same size and shape as the gel dosimeters, filled with gels of approximately the same concentration to simulate the induced inhomogeneities expected in the dosimeters.[33]

GafChromic film irradiations

An independent 2D dose assessment of the central slice of the "K" treatment plan was completed using EBT GafChromic film (International Specialty Products, NJ, USA). The "K" pattern was planned and delivered to an in-house built polystyrene phantom with the film placed at one of the seven possible plane positions, using the same tomotherapy benchtop and cobalt-60 irradiator as

in the gel irradiations described above.[26] The film was positioned at the central "K" slice and the delivery scaled down to 300 cGy. Twelve film samples were also irradiated to known doses from 0 to 8 Gy to establish the film optical density-to-dose calibration. An Expression 10000XL flat bed scanner (Epson Canada Ltd., Toronto, Canada) was used for film scanning.

Scatter perturbation assessment

Optical cone beam imaging of scattering media (such as the NIPAM polymer gel dosimeter) has been shown to be nonlinearly affected by angled scatter stray light perturbation that compromises the accuracy of absolute measurement.[17] However, the possibility exists that a well-behaved range of linear, *relative* scatter attenuation measurements could be established under some set of limiting conditions. To investigate this possibility, hybrid scattering acrylic emulsion–gelatin phantoms were manufactured in 1 L PETE jars using a similar approach to a previous investigation.[36] These phantoms separate the optical measurement from the uncertainties of dosimeter manufacture and dose delivery. For each phantom, a gelatin mixture was prepared by adding 5 wt% gelatin (Cat. No. G2500, Sigma-Aldrich Ltd.) to room temperature distilled, deionized water. The mixture was allowed to swell for 15 min at room temperature, heated to 45 °C, and held for 5 min at that temperature to dissolve the gelatin. A suitable quantity of propylene glycol was then added to the heated gelatin–water solution for refraction matching to a typical 6 %T NIPAM gel dosimeter recipe. After preparation, the heated propylene glycol–gelatin–water solution was poured into a 1 L PETE jar with a rigid finger-shaped container fixed in the jar to form the mould shape. The gel-filled jar was then placed in the refrigerator overnight to set the mould. On the following day, hot water at a temperature of 40–50°C was poured into the finger-shaped container, melting the gelatin mould slightly near the walls, and allowing the container to be removed. Calibration scattering solutions of varied concentration prepared according to Olding *et al.*[17] were poured into the mould cavity. This hybrid scattering acrylic emulsion-gelatin phantom was then imaged on the Vista scanner at each concentration of scattering solution.

To separate the optical scattering attenuation of the gelatin matrix from the other chemical components in the NIPAM gel dosimeter, a 5 wt% gelatin-in-water-filled PETE jar was imaged on the Vista scanner against a reference PETE jar containing matching tank solution. The phantom was prepared by adding the gelatin (Cat. No. G2500, Sigma-Aldrich Ltd.) to room temperature distilled, de-ionized water. The mixture was allowed to swell for 15 min and then heated to 45 °C for 5 min to dissolve the gelatin. The heated solution was poured into a PETE container and placed in the refrigerator overnight to set the gelatin. The gelatin-filled jar was then brought to room temperature conditions prior to optical scanning.

The contribution of reacted monomers in solution to background optical scatter attenuation was then considered. A reference scan was taken of a PETE jar filled with matching tank fluid. Data scans and corresponding optical CT images were then acquired for an unirradiated 6 %T dosimeter prepared according to procedure A (batch A2), and two unirradiated 4 %T dosimeters prepared according to: (a) procedure A (batch A3), and (b) the proposed alternative procedure B (batch B8).

Results

Initial optical CT-MRI comparison

In the optical CT-MRI comparison, the relationship between optical CT attenuation and dose was calibrated from the central slice in the "A" pattern dose distribution as shown in Figure 2a. The treatment plan dose and gel-measured attenuation patterns were first visually (manually) registered, and specific points covering the full dose-to-attenuation range were selected along the beam axes in the central slice of the "A" pattern. The dose and optical attenuation values at these points in the treatment plan dose and optical CT-measured attenuation distributions respectively were then fit to a linear relationship [Figure 2(b)]. The calibration relationship between attenuation (μ) and dose (D) was found to be $\mu = (0.00060 \pm 0.00002) D + (0.029 \pm 0.005)$ with an R^2 value of 0.977. A similar process was used for MRI $R2$-to-dose calibration, with the results also shown in Figure 2b. The relationship between relaxation rate ($R2$) and dose (D) was found to be $R2 = (0.00068 \pm 0.00002)D + (1.502 \pm 0.004)$ with an R^2 value of 0.997. The calibration relationships were then applied to the full dosimeter volumes imaged using optical CT and MRI. Figure 2c and d shows volume images of the treatment plan dose and optical CT measured attenuation distributions, respectively. The optical CT and MRI-measured data were found to have reconstructed mean-to-standard deviation signal-to-noise ratios (SNR) primarily in the range of 50–100 throughout the pencil beam dose regions. A $5 \times 5 \times 1$ voxel^3 region-of-interest located at different positions in the image volume was used to measure the SNR. Note that the initial, manual approach to optical dose-to-attenuation registration was later modified to improve the calibration methodology, as described in a latter section in this report.

Figures 3a and b presents two dimensional (2D) maps of a 3%, 3 mm Low's gamma function voxel-by-voxel comparison of gel-measured dose against the reference treatment plan dose in the central plane of the calibrated "K" pencil beam delivery, for cone beam optical CT and MRI dose readout respectively (batch A1). The 2D gamma evaluations were completed using an in-house developed software routine[37] based in the MATLAB environment (Mathworks, Newark, NJ, USA). Significant disagreement between treatment plan dose and gel-measured dose was observed over most of the central slice of the optical CT-

imaged "K' dose distribution, with only 60.2% of the voxels in agreement when using a generous 3%, 3 mm gamma criteria. In comparison, most of the voxels (92.8%) in the central slice of the MR-imaged "K" dose distribution were in agreement with treatment plan dose when the same gamma function criteria are applied. These results will be reviewed in the "Discussion" section.

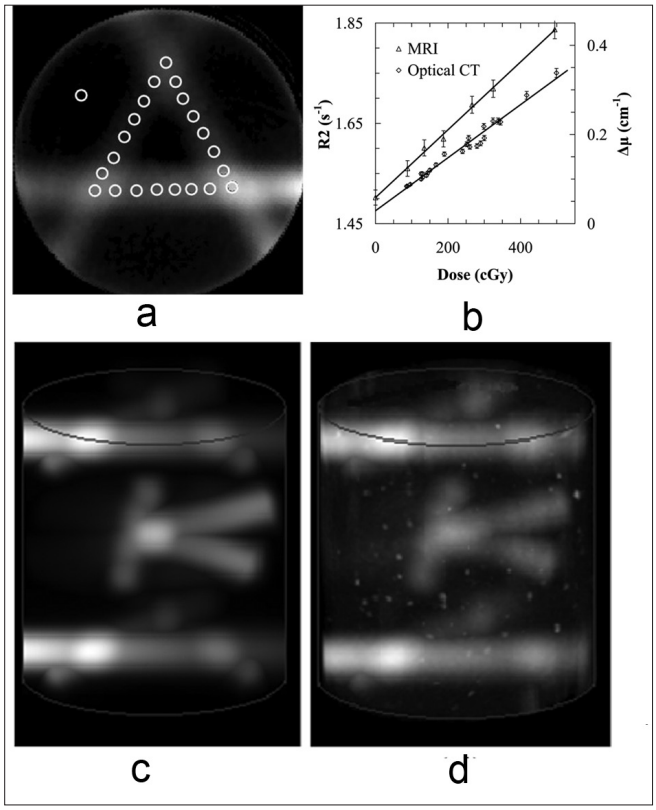

Figure 2: NIPAM gel dosimeters prepared according to procedure A were irradiated using (a) a standard pencil beam "A" pattern. (b) A calibration curve is obtained by registering and correlating well-determined points on the plan and optical CT slice. (c) A volume image of a treatment plan containing two calibration "A" patterns and one measurement "K" pattern, and (d) the corresponding NIPAM gel dosimeter-measured optical CT image.

Optical scatter perturbation assessment

Figure 4a–c shows projection images of 9.2 cm diameter PETE jar phantoms incorporating: (a) a gelatin matrix surrounding a 1.6 cm diameter scattering finger, (b) a gelatin matrix surrounding a 5 cm diameter scattering finger, and (c) a uniform scattering solution, acquired by the Vista scanner. The image data from the 1.6 cm diameter scattering finger phantom indicates linearity in mean attenuation value up to at least 0.6 cm^{-1} for a 1 cm diameter, 8 cm high cylindrical region-of-interest (ROI) centered in the scattering finger region [Figure 4d]. The image data from the 5 cm diameter scattering finger phantom displays nonlinearity at ~0.26 cm^{-1} for a 4 cm diameter, 8 cm high measurement ROI centered in the scattering finger region. Both of these upper limits well exceed that for the scattering solution-filled jar phantom at 0.125 cm^{-1} within an 8 cm diameter, 10 cm high measurement ROI centered in the jar volume.

In the evaluation of the sources of dosimeter background scatter attenuation, the mean attenuation of the 5 wt% gelatin-in-water matrix was found to be 0.030 ± 0.005 cm^{-1} in a preferred cylindrical ROI covering the central 8 cm in diameter (i.e., within 5 mm of the jar walls) and central 10 cm in height of the jar volume.[17] The ROI attenuations of the un-irradiated 6 %T and 4 %T dosimeters prepared according to procedure A were found to be 0.10 ± 0.02 cm^{-1} and 0.074 ± 0.008 cm^{-1}, respectively.

A reduced ROI background attenuation (0.050 ± 0.002

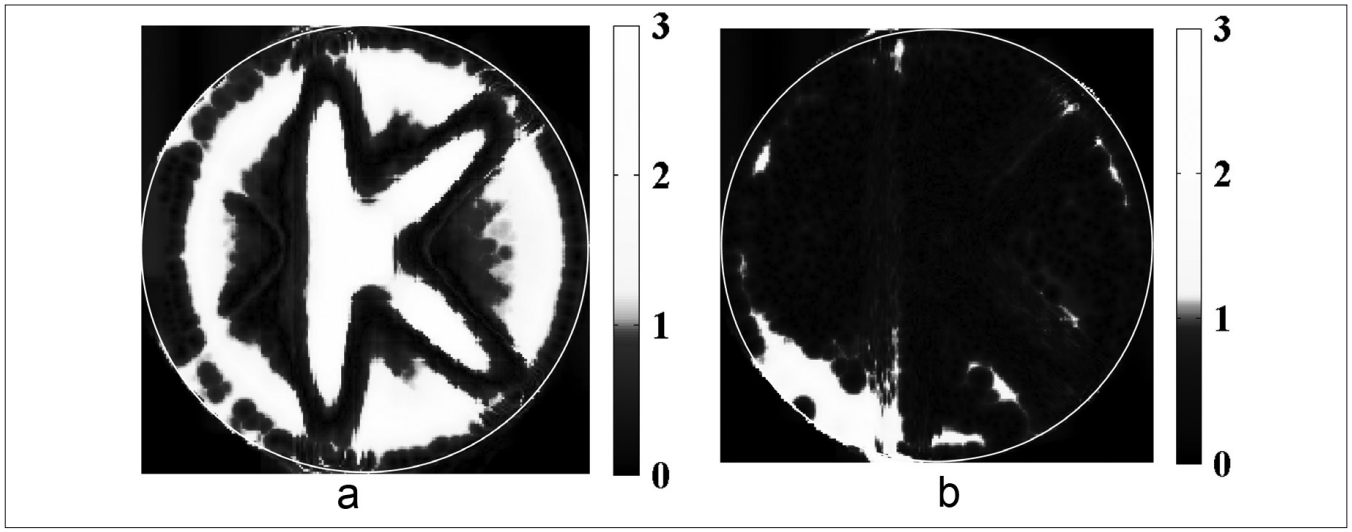

Figure 3: The central slice of a 500 cGy "K" treatment plan delivered to the 6 %T NIPAM gel dosimeter prepared according to procedure A was calibrated with the dose-to-attenuation relationship determined from the "A" pattern, and evaluated using a Low's gamma function analysis with 3% dose and 3 mm distance-to-agreement gamma function criteria. Two-dimensional gamma maps are shown comparing treatment plan dose to gel-measured dose obtained from (a) optical CT and (b) MR imaging

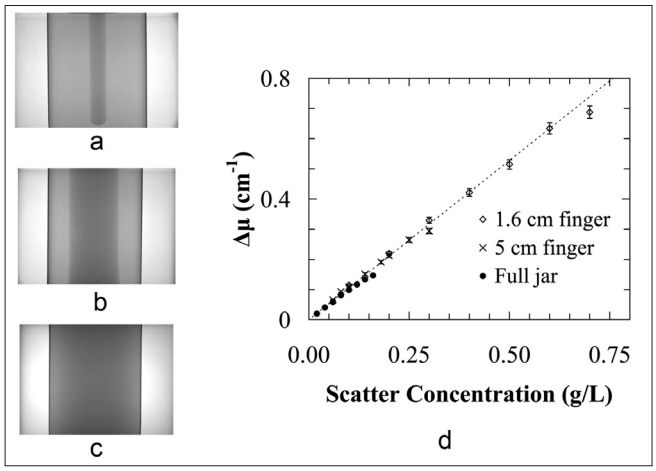

Figure 4: Vista scanner projection images from (a) a 1.6 cm diameter scattering finger-gelatin phantom, (b) a 5 cm diameter scattering finger-gelatin phantom, and (c) a scattering solution –filled jar phantom. (d) Vista mean attenuation value versus scatter concentration, measured within the scattering finger region-of-interest for the different phantoms, indicating the range of approximately linear behavior for each size of scattering region. Some of the error bars are smaller than symbol size

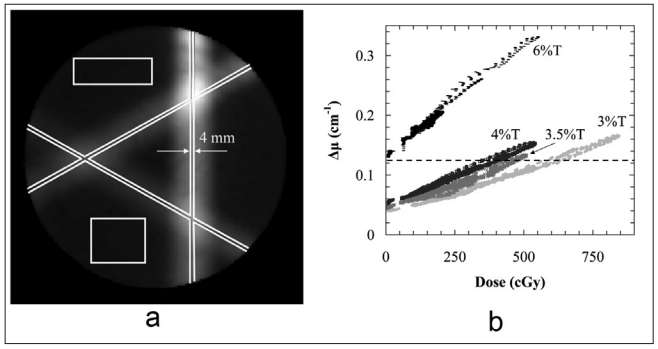

Figure 6: (a) The attenuation-to-dose calibration regions-of-interest for a 4 %T NIPAM-based dosimeter prepared according to procedure B and irradiated using a standard intersecting pencil beam "A" pattern. (b) Dose data from the central plane of calibration "A" patterns delivered to four NIPAM-based dosimeters prepared according to procedure B, with total monomer in the range of 3-6 %T. The dotted line indicates the approximate limit of well-behaved readout of well-characterized scattering solution-filled PETE jar dosimeters

cm^{-1}) was observed after the change in 4 %T dosimeter preparation to procedure B. Figure 5a and b shows vertical slices through the reconstructed optical CT images of the 6 %T and 4 %T dosimeters prepared according to procedure A (batches A2, A3). Figure 5c shows the same vertical slice through the optical CT image of the 4 %T dosimeter prepared according to procedure B (batch B8).

Dosimeter performance

Optical data from the central plane of calibration "A" patterns delivered to four NIPAM dosimeters (3 %T, 3.5 %T, 4 %T, and 6 %T) prepared according to procedure B (batches B1, B3–B5) are shown in Figure 6. The data were selected according to a modified calibration approach compared to that described in Figure 2a. Registration of gel-measured

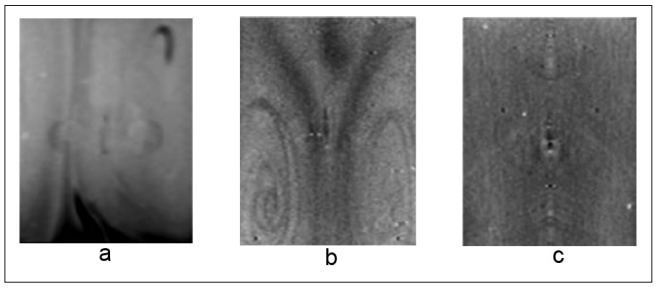

Figure 5: Reconstructed image data showing the qualitative variation in dosimeter background attenuation with manufacture procedure. Both the (a) 6 %T and (b) 4 %T dosimeters can have significant irregularities in dosimeter background. These irregularities and the overall background opacity can be reduced as seen in (c) a 4 %T dosimeter produced by a modified preparation method. The central axis artifacts seen in (c) are not features in the dosimeter but are related to other stray light effects from scanner imaging. The slice in (c) is windowed at a significantly higher level of contrast than (a) and (b) to show these artifacts

dose to treatment plan dose was accomplished using an automatic computer selected point based registration tool written in MATLAB.[37] This routine used a standard search algorithm to find the magnitude and spatial coordinates of the three peaks at the vertex points in the "A" pattern. The user selected the central planes in both the treatment plan dose and gel-measured attenuation distributions, the algorithm found the matching vertex points in both distributions, and then applied a rotation to the gel-measured data to align the vertex points of the two distributions. A larger number of data points (>3000) were used in the dose-to-attenuation second-order polynomial fit calibration, taken from the marked regions in Figure 6a. The dashed line shown in the plot [Figure 6b] indicates a mean attenuation value of 0.125 cm^{-1}, assessed as the point of significant departure from linearity of the scattering solution-filled PETE jar cone beam image data in the previous section [Figure 4d].

Figure 7a shows an evaluation of an irradiated 6 %T dosimeter prepared according to procedure B (batch B2). A 2%, 2 mm 2D Low's gamma function analysis of the central "K" slice calibrated with the "A" pattern-derived dose-to-attenuation relationship indicates significant disagreement between the plan and gel dose measurement, reporting only 50.3% voxel agreement within the specified criteria. A re-evaluation of the data in Figure 7a using a 3%, 3 mm gamma criteria indicates greater level of agreement (89.2%) than that reported in Figure 2a (60.2%). Hence, the results presented in Figure 7a represent an improvement over the initial optical CT results presented in Figure 2b. However, unacceptable regions of failure are still indicated in both high and low dose regions in the dosimetry, partially due to operation outside the approximate upper measurement limit of the Vista scanner.

When the experiment was repeated on a 4 %T dosimeter prepared according to procedure B (batch B3), an improved 92.7% voxel agreement is observed between treatment

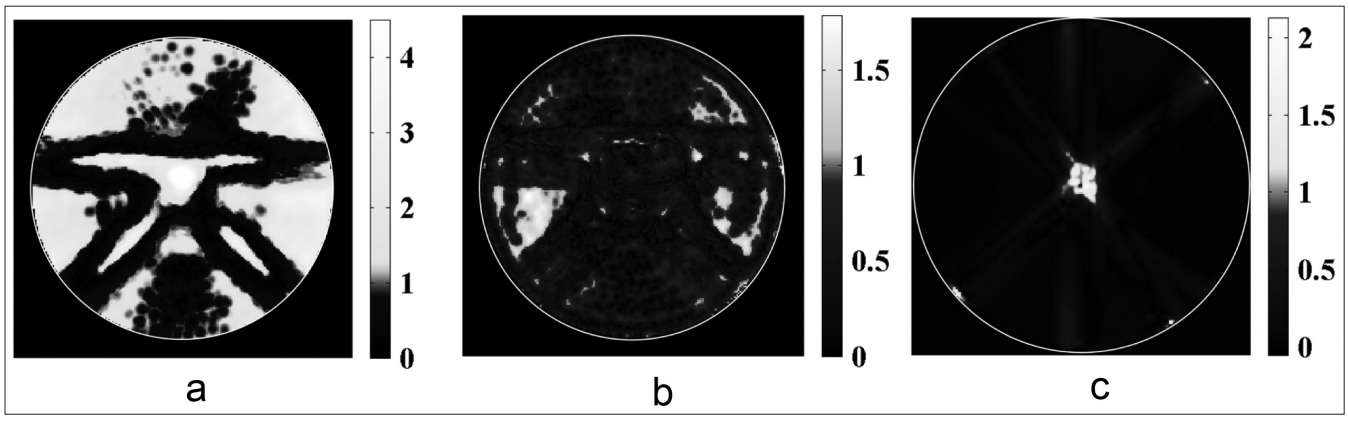

Figure 7: Low's gamma function evaluations (2%, 2 mm) of a 500 cGy "K" treatment plan (left) delivered to (a) a standard 6 %T dosimeter, (b) a 4 %T dosimeter and (c) GafChromic film

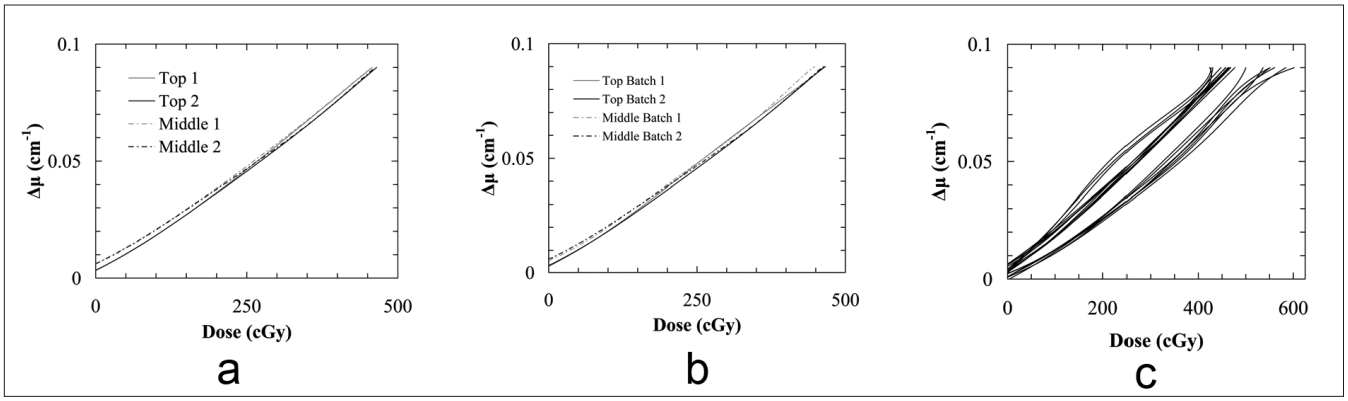

Figure 8: Second-order polynomial dose-to-attenuation fits to calibration "A" patterns delivered to two 4 %T NIPAM-based polymer gel dosimeters prepared (a) from the same gel batch, (b) on the same day from different gel batches, according to procedure B, and (c) from multiple batches prepared on different days using varied chemical lots

plan dose and gel-measured dose using 2%, 2 mm gamma comparison criteria [Figure 7b]. This level of gel performance is still not quite on par with, but is much closer to that of a 2D standard film measurement. A 2%, 2 mm 2D Low's gamma function analysis of the independent GafChromic film measurement shown in Figure 7c indicates 98.5% voxel agreement between treatment plan dose and film dose. Most of the observed failure in the central region was due to mechanical abrasion of the film.

In the evaluation of different calibration approaches, raw data were obtained from the central plane of each intersecting pencil beam irradiation according to the method in Figure 5a. The intra-batch dose response (i.e., response between two dosimeter jars prepared from the same gel batch B6) was investigated through calculation of second-order polymer fits to the "A" patterns in these jars, shown in Figure 8a. Note that the raw data were not shown in the plots shown in Figure 8, due to the resulting difficulty in differentiating and interpreting the overall dose response from the large number of overlapping raw data points (over 3000 points per calibration dataset). The fitted dose responses were found to be in agreement to within 3.6% of the dose maximum over the full dose range [Figure 8a]. The average difference between fits was 1.5%, falling within the combined standard error of the fits of ~4.0%.

The interbatch dose response was investigated in a similar manner. In this case, the polynomial fits to the "A" patterns in two dosimeter jars prepared from the different gel batches (B6 and B7) differed by as much as 3.8% [Figure 8b]. The average difference of 1.6% between fits was also within the combined standard error of the fits (~4.5%), and was only slightly worse than the result from intrabatch calibration. Both these gel batches were prepared on the same day using the same chemical lots. They were also irradiated and scanned within a short time period of each other. When the day of preparation, chemical lot, or irradiation and scan times are varied, the "A" pattern calibration fits varied considerably, as shown in Figure 8c (gel batches not numbered).

Discussion

Initial optical CT-MRI comparison

On preliminary examination, the calibration data in

Figure 2b indicates that the NIPAM dosimeter has a well-behaved linear dose response, without obvious stray light perturbation due to angled scatter signal. However, a 2D gamma function analysis of the optical CT-imaged (and "A" pattern–calibrated) "K" dose distribution [Figure 3a] reports an unacceptable level of disagreement between treatment plan dose and gel-measured dose in the central slice of the dose distribution. Without further investigation, these results seem to indicate that cone beam optical CT is unsuitable for readout of scattering polymer gel dosimeters.

The observed failure in optical CT imaging is consistent with results presented in a previous report indicating that, despite the conformation of the data to a linear fit, the Vista scanner scatter attenuation measurements exhibit nonlinear behavior compared to "true" spectrophotometer attenuation measurements.[17] This prior work concludes that artifacts arising from angled scatter and other forms of stray light perturbation compromise the accuracy of attenuation measurement over the entire volume of the scattering media-filled PETE jar dosimeter. The previous results show that the accuracy of the cone beam optical scatter measurement reduces significantly with increasing mean scatter attenuation within the 1 L PETE jar dosimeter [Figure 1a in Olding *et al.*[17]). A second conclusion from Olding *et al.*[17] was that angled scatter and other forms of stray light perturbation need to be better managed or corrected for in order for the combination of polymer gel dosimetry and cone beam optical CT imaging to be viable.

A large percentage of the disagreement observed in MR imaging [Figure 3b] can be attributed to susceptibility artifacts near the jar edge. Also, the 5 mm slice thickness in the z-direction leads to inaccuracy in the measurement due to volume averaging in the high gradient regions. Even with these limitations though, the MRI-measured data passed the 3%, 3 mm agreement criteria, indicating that the disagreement in the optical CT dose measurement [Figure 3a] was primarily related to failure in the readout and not in the dosimeter.

One final point to be made is that, due to time constraints, it was necessary to scan the irradiated dosimeter using MRI on a subsequent day to that of the optical CT imaging. However, since an in-jar (or intrajar) "A" calibration of attenuation-to-dose was performed for both readout modalities, and then applied to the "K" dose distribution, the differences in dosimeter scan temperature and dosimeter development time are well accounted for in the calibrated "K" dose distribution

Optical scatter perturbation assessment

Cone beam imaging data from the hybrid acrylic-gelatin scattering finger phantoms [Figure 4d] shows that the point at which the scanner scatter attenuation measurement significantly depart from linearity varies with the size and shape of the scattering region. The results also indicate that the relative attenuation measurements show reasonable linearity and reproducibility over a range of scatter concentrations and scattering region volumes. This range increases as the size of the scattering region decreases. A benchmark upper limit on the well-behaved linear fit range of (relative) scatter attenuation measurement for small field dose deliveries to a NIPAM-gel filled PETE jar dosimeter can, therefore, be roughly established as 0.125 cm^{-1}. This value represents the worst-case scenario, where the full PETE jar volume exhibits this scatter attenuation.

The goal, therefore, is to reduce the overall dosimeter response so that all post-irradiation attenuation values from the dosimeter fall within this well-behaved linear fit range of attenuation measurement. The simplest approaches to reduction of angled scatter-sourced stray light perturbation include increasing the scanner light source wavelength into the infrared and/or reducing the dose contrast sensitivity and scatter attenuation background of the NIPAM gel. Dosimeter modification was selected as the route of choice as it was easiest to adjust, and was estimated as being capable of greater reduction in stray light perturbation. Both routes involve a necessary trade-off of lower signal-to-noise ratio.

The reported mean attenuation values from the 5% gelatin-in-water-filled jar and a typical 6 %T dosimeter [Figure 5a] indicate that most of the background scatter attenuation in the dosimeter is not from the gelatin matrix. The remaining background scatter attenuation is likely sourced from independent polymerization reactions involving the BIS and NIPAM monomers. It is conceivable that a small reduction in background could be achieved by lowering the gelatin content in the dosimeter to 3–4 wt%. However, a larger reduction in background may be possible through better control of monomer reactions in solution, if there are monomer-based polymerization reactions occurring prior to irradiation.

Figure 5a and b shows the effect of lowering the total weight percentage of the NIPAM and BIS monomers from 6 %T to 4 %T. A corresponding decrease in background attenuation was observed in this experiment, supporting the conclusion that monomer polymerization is a second and major source of background scatter attenuation in the NIPAM polymer gel dosimeter. Both dosimeters [Figure 5a and b] were observed to have irregular backgrounds. This feature is likely due to thermal currents during spatial fixing of scattering particles in the gelation process. These irregular backgrounds can affect the accuracy of the gel dose measurement if the jar is slightly shifted between reference and data scans. Following this evaluation, our unpublished results from the testing of the BIS and NIPAM monomers indicated that the NIPAM monomer in particular may undergo some form of polymerization

reaction after the addition of THPC oxygen scavenger to a NIPAM–water mixture. This has been evidenced by a clear-to-cloudy reversible phase transition observed in the NIPAM–water–THPC solution as the temperature of solution is raised and lowered past the temperature range of 25–30 °C. This clear-to-cloudy reversible transition is consistent with reports in literature[38,39] describing the de-swelling behavior of polymerized NIPAM in solution at a lower critical solution temperature in the temperature range of 25–30 °C, accompanied by a measurable increase in turbidity. In basic polymer science literature, an initiator is generally used to cause polymerization of the NIPAM monomer in solution. In the case of the NIPAM–water–THPC mixture, the initiator is not known, but it may possibly be some combination of ultraviolet light exposure, chemical contaminants, or heat. There is some time hysteresis in this reversible temperature-dependent phase transition, such that de-swelled polymerized NIPAM in solution may remain as "frozen-in" scattering particles in the polymer gel dosimeter after it has transitioned to solid gel state under refrigeration. This is believed to be the source of the increase in scatter background with monomer addition. This conclusion is consistent with the results obtained when the gels are prepared with acrylamide monomer replacing the NIPAM monomer (but keeping the same BIS cross-linking monomer). The replacement of the NIPAM monomer with the acrylamide monomer leads to a lower polymer gel background scatter attenuation background of 0.05–0.06 cm^{-1} (unpublished results), much closer to that measured for the gelatin matrix. Unlike the NIPAM monomer, no evidence of lower critical solution temperature behavior is indicated for acrylamide in the literature.

To address this issue with the NIPAM monomer, a change was made to dosimeter preparation, as described in procedure B. The thought was that undesirable polymerization-deswelling behavior of the NIPAM monomer could mostly be avoided by dissolving NIPAM separately in room-temperature water, then adding THPC to this mixture at the last possible moment before addition of the NIPAM–THPC–water solution to the BIS–gelatin–water solution at 33–34 °C. This procedure yields a final solution temperature of approximately 30°C, which is sufficiently above the gelatin set point of roughly 26–28 °C so that the solution can be poured into the dosimeter jar without the formation of entrapped bubbles. The dosimeter jar is immediately placed in a dark refrigerator to prevent the suspected UV light initiation of polymerization.

As seen in Figure 5, the change in preparation approach (to procedure B) advantageously reduces both the irregularities and the overall level of the dosimeter background scatter attenuation from around 0.075 ± 0.008 cm^{-1} [Figure 5b] to as little as 0.050 ± 0.002 cm^{-1} for a 4 %T NIPAM-based polymer gel dosimeter [Figure 5c]. The reduced background attenuation of the 3–4 %T polymer gels, combined with the lower irradiation gel dosimeter sensitivity, then results in irradiated dosimeter attenuation values that are below the approximated upper limit on mean jar scatter attenuation linearity from the cone beam optical CT scanner [Figure 6b].

To be clear, the overall message from Figures 4–6 is not that scatter-based stray light perturbation has a negligible effect on the dose accuracy in the full 3D volume below the approximate scanner measurement limit shown in Figure 6b. Rather, the data presented in Figure 4b indicate that the readout within the small volume, high-scatter attenuation field regions (i.e., within the central 1 cm diameter of the 1.6 cm diameter finger) is linear up to approximately 0.6 cm^{-1} as long as the background stays constant. However, the readout in the lower scattering regions outside these highly scattering (high dose) regions may be contaminated by scatter signal originating from the high dose regions.

Modification of the cone beam scanner's area light source in the scanner to a fast scanning, fan beam collimated light source would be one logical approach to further reducing the scatter perturbation and improving in the measurement accuracy of this system. This approach would compromise between the fast scan time of the cone beam scanner configuration and the improved scatter rejection of point-detection laser beam-photodiode optical scanners. The fan beam route is anticipated to be a viable option for imaging polymer gels, since these dosimeters are relatively unaffected by spatial dose degradation over time (due to diffusion).

Dosimeter Performance

The gamma function analyses presented in Figure 7 indicate that the cone beam optical CT-based NIPAM gel dosimetry is improved after modification of the dosimeter formulation and preparation procedure. However, the best results from the use of the 4 %T NIPAM gel-filled dosimeter fall short of the preferred goal of full (or near full) agreement between treatment plan and gel-measured dose distributions using 2% dose and 2 mm distance-to-agreement gamma function criteria. The NIPAM gel measurement is also slightly less accurate than the film measurement. This drawback is arguably outweighed by the benefit of having 3D gel dose data compared to the 2D film dose data.

One possible source of the disagreement observed in the low dose regions of the gel measurement in Figure 7b may be scatter-derived stray light perturbation arising from the high dose, high scattering regions of the irradiated pencil beams, as contemplated in the previous discussion

section. Another source is the uncertainty related to the calibration of attenuation-to-dose from the "A" pattern dose distribution which incorporates spatial uncertainties from the setup and dose delivery. The change in calibration methodology (from Figure 2a to Figure 6a with consequent increased data collection) reduces the uncertainty on the calibration fit from the order of 3%–2%, but this would preferably be lower yet. The setup uncertainties would be less of an issue if, for example, an electron beam central axis depth dose were used for calibration. However, the preferred larger electron beam field size (4 cm or greater) for accurate dose measurement would introduce a greater scatter volume and hence, more scatter perturbation affecting the accuracy of the measurement. For this reason, the use of the "A" pattern pencil beam delivery was felt to be the best approach for attenuation-to-dose calibration from cone beam optical CT-based NIPAM gel dosimetry, despite the acknowledged setup uncertainties affecting the accuracy of the dose calibration relationship [Figure 2b]. These uncertainties cannot be directly correlated to the results from the gamma analysis, but will be a limiting factor affecting the measurement [Figures 3 and 7]. However, the high level of agreement observed between the treatment plan and film measurement in Figure 7c suggests that the uncertainties in Figure 2b related to setup of the tomotherapy apparatus and pencil beam plan delivery are less significant in the calibration of gel attenuation to dose than those related to gel readout (i.e., gel response, background irregularities, scatter perturbation, etc.). The presence of ringing artifacts due to contaminant imperfections such as foreign particles in the gel is a third source of disagreement (see circular streak high gamma value regions in Figure 7b).

Even with these limitations, the results presented in this work indicate that (1) an improved dosimeter preparation procedure, and (2) better matching of the dosimeter and scanner performance capabilities, lead to a significant improvement in the accuracy of small field dose delivery evaluations using cone beam optical CT-based NIPAM gel dosimetry. While the limitations on what constitutes a small field have not strictly been specified, the results from this study suggest that the assessment of pencil beam deliveries of 1–2 cm field width may be possible using the standard-sized 4 %T NIPAM dosimeter if anticipated future improvements (reducing stray light perturbation in the imaging) are realized.

The in-jar calibration approach used for most of the dose delivery assessments in this investigation is limited in its application to select planar deliveries; an interjar calibration approach would be necessary for most practical dose delivery evaluations. The results from Figure 8a demonstrate that a same-batch, interjar calibration methodology for the evaluation of small field dose deliveries using cone beam optical CT-based NIPAM gel dosimetry may be feasible, albeit with some reduction in accuracy related to the uncertainties of gel preparation. It was expected that using a "calibration" and a "measurement" dosimeter prepared from the same gel batch, in the same container size, and under the same environmental conditions[40] would clearly be the best approach. The approximately equivalent performance from inter-batch dosimeter calibration when the batches were prepared on the same day [Figure 8b] was a surprising result. However, only a single set of experimental results are presented in each of Figure 8a and b, so definitive conclusions cannot be drawn in this regard.

Conclusions

The measurement accuracy of cone beam optical computed tomography-based NIPAM polymer gel dosimetry is improved through modification of the dosimeter formulation and preparation procedure to better match the dosimeter attenuation background and dose sensitivity to the imaging capabilities of the scanner. However, the gel measurement did not achieve the target goal of full (or near to full) high-resolution voxel agreement between the well-characterized pencil beam plan dose and gel-measured dose distributions for 2% dose and 2 mm distance-to-agreement gamma comparison criteria. Further improvements will be required in order for this system to be a viable tool for evaluation of small field dose deliveries. Babic *et al.*[18] have contemplated the evaluation of small field deliveries with optical cone beam Fricke gel dosimetry and have established the measurement with corrections for diffusion. Similarly, the work in this report indicates that small field deliveries may also be evaluated using optical cone beam polymer gel dosimetry, but that a correction strategy will be required to address the effects of scatter perturbation. Both intrabatch and interbatch calibration may be suitable for establishing the dose response of the polymer gel, but inter-batch calibration will require additional attention to the chemical lot, manufacture and environmental conditions of the dosimeter prior to irradiation.

Acknowledgements

Research funding for this work has been provided by the Cancer Centre of Southeastern Ontario, the Ontario Research and Development Fund (OCITS Consortium), and the Canadian Institutes of Health Research (CIHR).

References

1. Gore JC, Kang YS, Schulz RJ. Measurement of radiation dose distributions by nuclear magnetic resonance (NMR) imaging. Phys Med Biol 1984;29:1189-97.
2. Olsson LE, Fransson A, Ericsson A, Mattsson S. MR imaging of absorbed dose distributions for radiotherapy using ferrous sulphate

gels. Phys Med Biol 1990;35:1623-31.
3. Gore JC, Ranade M, Maryanski MJ, Schulz RJ. Radiation dose distributions in three dimensions from tomographic optical density scanning of polymer gels: I. Development of an optical scanner. Phys Med Biol 1996;41:2695-704.
4. Hilts M, Audet C, Duzenli C, Jirasek A. Polymer gel dosimetry using x-ray computed tomography: A feasibility study. Phys Med Biol 2000;45:2559-71.
5. Jirasek A, Hilts M, McAuley KB. Polymer gel dosimeters with enhanced sensitivity for use in x-ray CT polymer gel dosimetry. Phys Med Biol 2010;55:5269-81.
6. Oldham M, Siewerdsen JH, Kumar S, Wong J, Jaffray DA. Optical-CT gel-dosimetry I: Basic investigations. Med Phys 2003;30:623-34.
7. Oldham M, Kim L. Optical-CT gel-dosimetry. II: Optical artifacts and geometrical distortion. Med Phys 2004;31:1093-104.
8. Doran S, Krstajic N. The history and principles of optical computed tomography for scanning 3-D radiation dosimeters. J Phys: Conf Ser 2006;56:45-57.
9. Doran S. The history and principles of optical computed tomography for scanning 3-D radiation dosimeters: 2008 update. J Phys: Conf Ser 2009;164:98-119.
10. Babic S, Battista J, Jordan K. Three-dimensional dose verification for intensity-modulated radiation therapy in the radiological physics centre head-and-neck phantom using optical computed tomography scans of ferrous xylenol-orange gel dosimeters. Int J Radiat Oncol Biol Phys 2008;70:1281-91.
11. Wolodzko JG, Marsden C, Appleby A. CCD imaging for optical tomography of gel radiation dosimeters. Med Phys 1999;26:2508-13.
12. Doran SJ, Koerkamp KK, Bero MA, Jenneson P, Morton EJ, Gilboy WB. A CCD-based optical CT scanner for high-resolution 3D imaging of radiation dose distributions: Equipment specifications, optical simulations and preliminary results. Phys Med Biol 2001;46:3191-213.
13. Krstajic N, Doran SJ. Focusing optics of a parallel beam CCD optical tomography apparatus for 3D radiation gel dosimetry. Phys Med Biol 2006;51:2055-75.
14. Krstajic N, Doran SJ. Characterization of a parallel-beam CCD optical-CT apparatus for 3D radiation dosimetry. Phys Med Biol 2007;52:3693-713.
15. Baldock C, Harris PJ, Piercy AR, Healy B. Experimental determination of the diffusion coefficient in two-dimensions in ferrous sulphate gels using the finite element method. Australas Phys Eng Sci Med 2001;24:19-30.
16. Olsson LE, Westrin BA, Fransson A, Nordell B. Diffusion of ferric ions in agarose dosimeter gels. Phys Med Biol 1992;37:2243-52.
17. Olding T, Holmes O, Schreiner LJ. Cone beam optical computed tomography for gel dosimetry I: Scanner characterization. Phys Med Biol 2010;55:2819-40.
18. Babic S, McNiven A, Battista J, Jordan K. Three-dimensional dosimetry of small megavoltage radiation fields using radiochromic gels and optical CT scanning. Phys Med Biol 2009;54:2463-81.
19. Maryanski MJ, Gore JC, Kennan RP, Schulz RJ. NMR relaxation enhancement in gels polymerized and cross-linked by ionizing radiation: A new approach to 3D dosimetry by MRI. Magn Reson Imaging 1993;11:253-8.
20. Maryanski MJ, Zastavker YZ, Gore JC. Radiation dose distributions in three dimensions from tomographic optical density scanning of polymer gels: II. Optical properties of the BANG polymer gel. Phys Med Biol 1996;41:2705-17.
21. DeJean P, Senden RJ, McAuley KB, Rogers M, Schreiner LJ. Initial Experience with a commercial cone beam CT unit for polymer gel dosimetry I: Optical dosimetry issues. Journal of Physics: Conf Ser 2006;56:179-82.
22. DeJean P, Senden RJ, McAuley KB, Rogers M, Schreiner LJ. Initial Experience with a commercial cone beam CT unit for polymer gel dosimetry II: Clinical potential. J Phys: Conf Ser 2006;56:183-6.
23. Low DA, Dempsey JF, Venkatesan R, Mutic S, Markman J, Haacke EM, *et al*. Evaluation of Polymer gels and MRI as a 3-D dosimeter for intensity-modulated radiation therapy. Med Phys 1999;26:1542-51.
24. Low DA, Dempsey JF. Evaluation of the gamma dose distribution comparison method. Med Phys 2003;30:2455-64.
25. Senden RJ, De Jean P, McAuley KB, Schreiner LJ. Polymer gel dosimeters with reduced toxicity: A preliminary investigation of the NMR and optical dose-response using different monomers. Phys Med Biol 2006;51:3301-14.
26. Dhanesar S. Conformal Radiation Therapy with Cobalt-60 Tomotherapy. M.Sc. Thesis, Kingston, ON, Canada: Queen's University.
27. Milan J, Bentley RE. The storage and manipulation of radiation dose data in a small digital computer. Br J Radiol 1974;47:115-21.
28. De Deene Y, De Wagter C. Artefacts in multi-echo T2 imaging for high-precision gel dosimetry: III. Effects of temperature drift during scanning. Phys Med Biol 2001;46:2697-711.
29. Graumann R, Oppelt A, Stetter E. Multiple-spin-echo imaging with a 2D Fourier method. Magn Reson Med 1986;3:707-21.
30. Baldock C, Lepage M, Back SA, Murry PJ, Jayasekera PM, Porter D, *et al*. Dose resolution in radiotherapy polymer gel dosimetry: Effect of echo spacing in MRI pulse sequence. Phys Med Biol 2001;46: 449-60.
31. De Deene Y, Baldock C. Optimization of multiple spin-echo sequences for 3D polymer gel dosimetry. Phys Med Biol 2002;47:3117-41.
32. Lepage M, Jayasakera PM, Back SA, Baldock C. Dose resolution optimization of polymer gel dosimeters using different monomers. Phys Med Biol 2001;46:2665-80.
33. Nkongchu K. Magnetic resonance imaging approaches to gel dosimetry for validation of conformal radiotherapy treatment plans. Ph.D. Thesis. Ottawa, ON, Canada: Carleton University.
34. Chang H, Fitzpatrick JM. A technique for accurate magnetic resonance imaging in the presence of field inhomogeneities. IEEE Trans Med Imaging 1992;11:319-29.
35. Kawanaka A, Takagi N. Estimation of static magnetic field and gradient fields from NMR image. J Phys E: Sci Instrum 1986;19: 871-5.
36. Bosi S, Naseri P, Puran A, Davies J, Baldock C. Initial investigation of a novel light-scattering gel phantom for evaluation of optical CT scanners for radiotherapy gel dosimetry. Phys Med Biol 2007;52: 2893-903.
37. Holmes, O Validation of Conformal Radiation Therapy Treatments in 3D Using Polymer Gel Dosimeters and Optical Computed Tomography. M.Sc. Thesis. Kingston, ON, Canada: Queen's University.
38. Kara S, Sayil C, Okay O. Real time temperature and photon transmission measurements for monitoring phase separation during the formation of Poly(*N*-isopropylacrylamide) Gels. J Appl Polym Sci 2002;86:3589-95.
39. Takata S, Suzuki K, Norisuye T, Shibayama M. Dependence of shrinking kinetics of poly(N-isopropylacrylamide) gels on preparation temperature. Polymer 2002;43:3101-7.
40. De Deene Y, Pittomvils G, Visalatchi S. The influence of cooling rate on the accuracy of normoxic polymer gel dosimeters. Phys Med Biol 2007;52:2719-28.

Source of Support: Cancer Centre of Southeastern Ontario, the Ontario Research and Development Fund (OCITS Consortium), and the Canadian Institutes of Health Research (CIHR)., **Conflict of Interest:** None declared.